A NEW STELLAR ATMOSPHERE GRID AND COMPARISONS WITH *HST/STIS* CALSPEC FLUX DISTRIBUTIONS

Ralph C. Bohlin[1], Szabolcs Mészáros[2,3], Scott W. Fleming[1], Karl D. Gordon[1,4], Anton M. Koekemoer[1], and József Kovács[2]

ABSTRACT

The Space Telescope Imaging Spectrograph (STIS) has measured the spectral energy distributions (SEDs) for several stars of types O, B, A, F, and G. These absolute fluxes from the CALSPEC database are fit with a new spectral grid computed from the ATLAS-APOGEE ATLAS9 model atmosphere database using a chi-square minimization technique in four parameters. The quality of the fits are compared for complete LTE grids by Castelli & Kurucz (CK04) and our new comprehensive LTE grid (BOSZ). For the cooler stars, the fits with the MARCS LTE grid are also evaluated, while the hottest stars are also fit with the NLTE Lanz & Hubeny OB star grids. Unfortunately, these NLTE models do not transition smoothly in the infrared to agree with our new BOSZ LTE grid at the NLTE lower limit of T_{eff}=15,000K.

The new BOSZ grid is available via the Space Telescope Institute MAST archive and has a much finer sampled IR wavelength scale than CK04, which will facilitate the modeling of stars observed by the James Webb Space Telescope (JWST). Our result for the angular diameter of Sirius agrees with the ground-based interferometric value.

Subject headings: stars: atmospheres — stars: fundamental parameters — techniques: spectroscopic

[1]Space Telescope Science Institute, 3700 San Martin Drive, Baltimore, MD 21218, USA

[2]ELTE Gothard Astrophysical Observatory, H-9700 Szombathely, Szent Imre Herceg St. 112, Hungary

[3]Premium Postdoctoral Fellow of the Hungarian Academy of Sciences

[4]Sterrenkundig Observatorium, Universiteit Gent, Gent, Belgium

1. INTRODUCTION

Stellar standards with accurate absolute fluxes (irradiance) are required for the calibration of the James Webb Space Telescope (JWST) and for the interpretation of dark energy measures with the supernova Ia technique. The JWST instrumentation and wavelength coverages include the Mid-Infrared Instrument (MIRI 4.9–28.8 μm), the Near-Infrared Camera (NIRCAM 0.6–5μm), the Near-Infrared Spectrometer (NIRSPEC 0.6–5.3 μm), and the Near-Infrared Imager and Slitless Spectrograph (NIRISS 0.6–5 μm).

The basis of the calibrated HST absolute fluxes is the set of three spectral energy distributions (SEDs) of NLTE model atmospheres for the pure hydrogen white dwarfs (WDs), GD153 and GD71, and a NLTE metal line-blanketed model of Rauch et al. (2013) for G191B2B (Bohlin 2014; Bohlin et al. 2014; Bohlin & Proffitt 2015). The STIS net signal in electrons/s from each of these primary standard WDs relative to the STIS net signal for Vega at 5557.5 Å (5556 Å in air) defines the absolute normalization of each model flux. Bohlin (2014) reconciled the 5557.5 Å Megessier (1995) flux value with the MSX 8–21 μm fluxes of Price et al. (2004) to establish the absolute flux of 3.44×10^{-9} erg cm^{-2} s^{-1} Å^{-1} for Vega at 5557.5 Å. In the IR, an additional primary standard is the special Kurucz model for Sirius, which fits both the 5557.5 Å and the average of the MSX measured fluxes to 0.5% (Bohlin 2014).

The spectral energy distributions of these three primary WDs establish the calibration of all the HST instruments, including the STIS and NICMOS spectrophotometers. Model atmospheres can then be fit to HST spectrophotometry for secondary flux standards; and these model fluxes establish a set of SEDs for calibrating JWST at IR wavelengths longer than the 1 μm STIS cutoff or the 2.5 μm NICMOS limit. (See Tables 5 and 6 for the list of our JWST standards and for the results discussed in Section 5.) Previously, Bohlin & Cohen (2008) fit the Castelli & Kurucz (2003, CK04) grid to A stars, and Bohlin (2010, B10) fit STIS and NICMOS fluxes for G stars with both CK04 and MARCS (Gustafsson et al. 2008) grids. The stars from these earlier works are re-fit here because of updated fluxes, improved techniques, and our new model grid.

The MARCS grid does not cover effective temperatures ($T_{\rm eff}$) above 8000 K; so another grid is required for comparison with the CK04 results. For our hottest stars, the Lanz NLTE grid (Lanz & Hubeny 2003, 2007) is appropriate, because the difference between LTE and NLTE becomes significant above ∼15,000 K. Our new grid that is discussed in Section 2 provides full coverage of our complete sample of stars; and Section 3 details the instructions for accessing the new grid. Section 4 explains our methodology and highlights some of our general results, while Section 5 illuminates the pros and cons of the separate grids. Section 6 summarizes some of the improvements of our new model SEDs, named BOSZ, using some

letters from the names of the first two authors. Model SEDs from this new BOSZ grid are available via the Mikulski Archive for Space Telescopes (MAST) at the STScI[1]. For each star, the best fitting BOSZ model at the full resolution of R=300,000 is extracted from our BOSZ grid, normalized to the observed SED, and placed in the CALSPEC database[2] along with a separate file containing the observed SED. From the long wavelength limit of the STIS or NICMOS data to 32 μm, this second CALSPEC file is a concatenation of the observed HST SED with the best fit R=500 model from our new BOSZ grid and is most appropriate for calibration of low resolution (R $\lesssim$ 500) data. Table 1 compares the four sets of model atmosphere grids that are used in this paper.

2. THE NEW GRID

A publicly available and consistently calculated database of model SEDs is important for many astrophysical analyses, including spectroscopic surveys and analysis of elemental composition of stellar atmospheres. Different spectral grids are available in the literature, and one of the largest is based on ATLAS9 Kurucz (1979) calculations (Zwitter et al. 2004) for the GAIA mission. More recently, Coelho (2014) published a synthetic spectral grid containing 12 compositions covering the metallicity range $[M/H] = \log z$ of -2.77 to -1.31, where z is the abundance ratio to hydrogen by number of the total sum of all elements except helium and hydrogen. These metal abundances are relative to the solar abundances of Asplund et al. (2005), where a model with $[M/H] = 0$ has the solar abundance. Other libraries of model atmosphere grids are also available in the literature; for a complete list, see the introduction by Coelho (2014). Older ATLAS9 libraries were synthesized using the solar reference abundance table from either Grevesse & Sauval (1998), or Anders & Grevesse (1989) and are limited to a handful of mixtures. However, in the early 2000s, significant changes and improvements were made to the solar compositions table (Asplund et al. 2005; Grevesse et al. 2007; Asplund et al. 2009) that should be used to calculate grids of updated stellar spectra. Two extensive modern grids, CK04 and MARCS, use the Grevesse & Sauval (1998) and (Grevesse et al. 2007) abundance tables, respectively.

Recently, Mészáros et al. (2012) calculated ATLAS9 LTE model atmospheres for a larger number of compositions. Using a 2 km/s microturbulent velocity, this grid covers metallicities from [M/H]=−5.0 to [M/H]=+1.0 with carbon ([C/M]) and α ([α/M]) abundances from −1.5 to +1.0 relative to solar metallicity. The α elements (i.e. those with an even

[1]`https://archive.stsci.edu/prepds/bosz`

[2]http://www.stsci.edu/hst/observatory/crds/calspec.html

Table 1. Parameters of the Full Model Grids

parameter	BOSZ	CK04[a]	MARCS	Lanz[d]
Type	LTE	LTE	LTE	NLTE
Wavelength range (μm)	0.1 – 32	0.09 – 160	0.13 – 20	0.0045 – 300
$T_{\rm eff}(K)$	3500 – 30,000	3500 – 50,000	2500 – 8000	15,000 – 55,000
log g	0 – 5 See Table 2	0 – 5 See CK04	-1 – 5[b]	1.75 – 4.75[e]
$[M/H] = \log z$	-2.5 to 0.5	-2.5 to 0.5	-5 to 1[c]	-1 to 0.3
$[C/M]$	-0.75 to 0.5	0	0[f]	0
$[\alpha/M]$	-0.25 to 0.5	0, +0.4	0[f]	0
Solar Abundance	Asplund et al. (2005)	Grevesse & Sauval (1998)	Grevesse et al. (2007)	Grevesse & Sauval (1998)
Microturbulent velocity (km/s)	2	2	0,1,2,5	2 ($\leq$30,000K),10($\geq$32,500K)
Rotational broadening (km/s)	0	0	0	0
Spectral resolution R	R=200–300,000[g]	1221 bins	R=20,000	R$\sim$1800
Convective mixing length	1.25	1.25	1.5	No convection
Convective overshoot	No	No	No	No convection
Continuum	Yes	Yes	No	No

[a]As updated from http://wwwuser.oats.inaf.it/castelli/.

[b]Models are plane-parallel, except sphericial below log $g = 3$. There are many missing models due to convergence problems, especially for the spherical cases. For example, 52 missing models are filled by interpolation in the plane-parallel set.

[c]Marcs models have a somewhat different definition of $[M/H]$, so that metallicity results for MARCS are not directly comparable to the other model results.

[d]As provided in the merged Cloudy format file obstar_merged_3d.ASCII from http://nova.astro.umd.edu/Tlusty2002/tlusty-frames-cloudy.html.

[e]See Lanz & Hubeny (2003) and Lanz & Hubeny (2007) for details.

[f]See Gustafsson et al. (2008) and http://marcs.astro.uu.se for details.

[g]The BOSZ model grid offers 10 choices in the R=200–300,000 range.

Table 2. Atmospheric Parameters of ATLAS9 Spectra

Parameter	Min	Max	Step	Parameter	Min	Max	Step
[M/H]	−2.5	0.5	0.25				
[C/M]	−0.75	0.5	0.25				
[α/M]	−0.25	0.5	0.25				
$T_{\rm eff}$	3500	6000	250	log g	0	5	0.5
$T_{\rm eff}$	6250	8000	250	log g	1	5	0.5
$T_{\rm eff}$	8250	12000	250	log g	2	5	0.5
$T_{\rm eff}$	12500	20000	500	log g	3	5	0.5
$T_{\rm eff}$	21000	30000	1000	log g	4	5	0.5

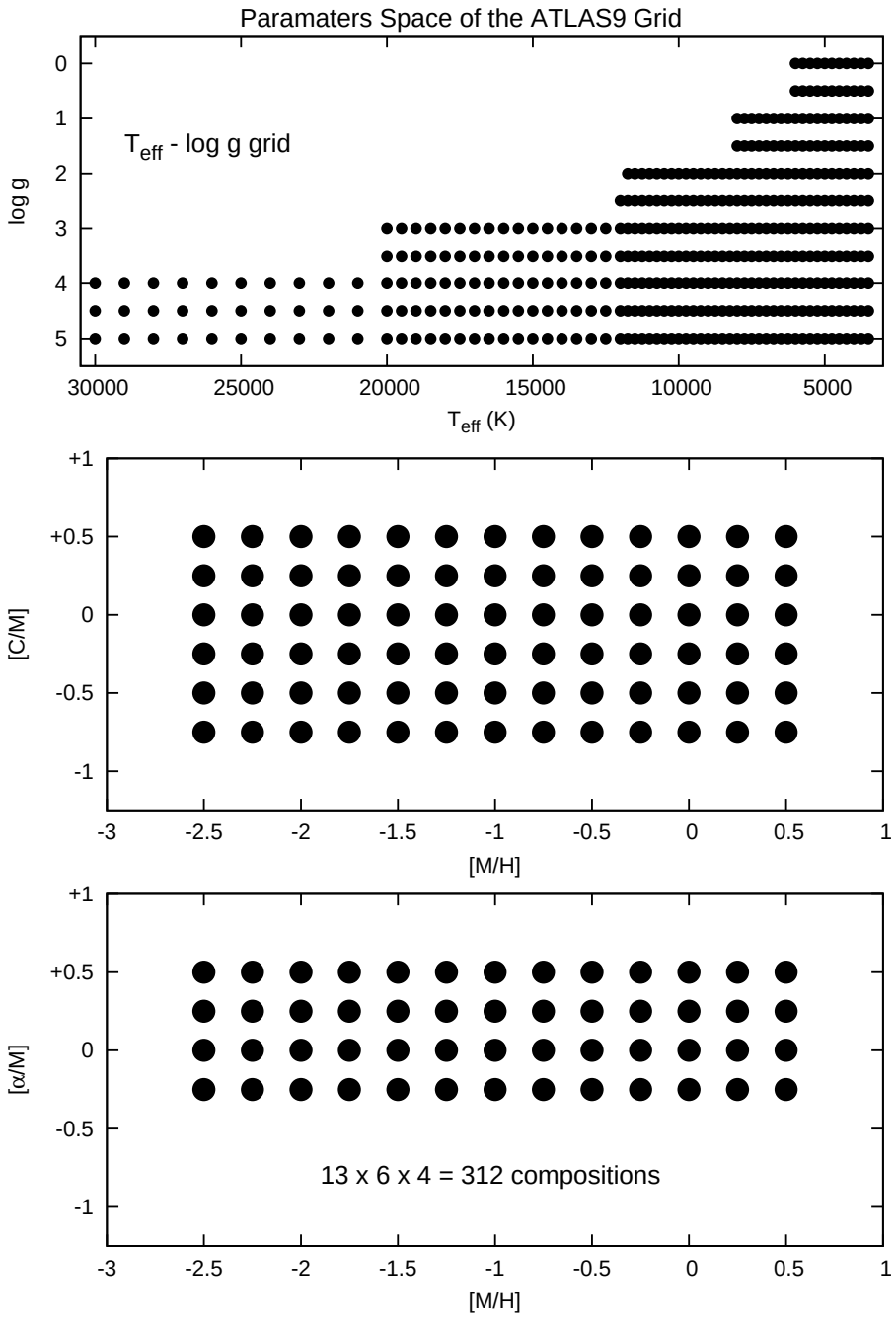

Fig. 1.— Top panel: The $T_{\rm eff} - \log$ g space of model atmospheres used for synthesis. Middle panel: [C/M] abundances as a function of metallicity. Bottom panel: [α/M] abundances for each [C/M] values as a function of metallicity. The product of our 13 [M/H], 6 [C/M], and 4 [α/M] values comprises the full parameter space of the 312 compositions.

number of protons) that are varied in these calculations are O, Ne, Mg, Si, S, Ca, and Ti. One of the most important differences between Mészáros et al. (2012) and previous model atmosphere grids is the use of more recent Solar abundances from Asplund et al. (2005); but the Mészáros et al. (2012) output grid SEDs contain only 333 wavelength points.

This plane-parallel dataset of Mészáros et al. (2012) is the model atmosphere grid for spectral synthesis of a new library that spans most of the atmospheric parameter space that is known to exist for actual stars. Atlas9 is chosen, instead of the available Atlas12 Kurucz code, because of the large variety of compositions in the grid and because Atlas12 requires more computation time and often fails to converge. The high-resolution spectra are calculated from the Mészáros et al. (2012) model atmosphere grid with SYNTHE (Kurucz & Avrett 1981) using the Linux-ported version (Sbordone et al. 2004). The selected atmospheric parameters are listed in Table 2 and shown in Figure 1. With a total of 312 different compositions that are selected to cover the majority of actual stellar abundances, our 13 [M/H], 6 [C/M], and 4 [α/M] values are a subset of the original Mészáros et al. (2012) grid. The spectra span the wavelength range of 1000 Å – 32 μm using vacuum wavelengths and are first synthesized with one sample point per resolution element at R = 300,000 without convective overshooting and with a mixing length parameter of 1.25. Lower-resolution spectra are produced by convolving the highest resolution SED with Gaussian line-spread functions of full-width-at-half-maximum λ/R. Nine additional resolutions are provided with two points per resolution element: R = 100,000, 50,000, 20,000, 10,000, 5,000, 2,000, 1,000, 500, and 200. The computed fluxes are sampled evenly in logarithmic wavelength space with a sample spacing of $\lambda/2R$ for two points per resolution element, and all SEDs with the same resolution have the same common set of wavelengths. No rotational broadening is applied to any of the models, while the 2 km/s micro-turbulent velocity is the same as used in the model atmosphere computation. Details of the naming convention for the MAST models are in the Appendix.

The atomic line list compiled by Robert Kurucz[3] is used without modification and is complemented with the molecular line lists for H_2O, CH, MgH, NH, OH, SiH, H_2, C_2, CN, CO, SiO, and TiO[4]. These line lists are frequently updated, but the April 2015 version is used for all the calculations. The H_2O Partridge & Schwenke (1997) and TiO Schwenke (1998) line lists were formatted for ATLAS9 by Robert Kurucz. Water is included for stars cooler than 5500 K and TiO only below 4500 K to reduce computation time for temperatures where these molecules are unimportant. The computations are parallelized by composition. Each

[3]http://kurucz.harvard.edu/linelists.html

[4]http://kurucz.harvard.edu/molecules.html

composition has 61 different temperatures and 3–11 different gravities according to Table 2, i.e. 415 models per composition and 312*415=129480 total models. Each model SED is available at the 10 different spectral resolutions for a total of 4150 files per composition and a grand total of 1.3 million files in the complete BOSZ grid.

3. THE GRID ARCHIVE

Each model SED has three columns: wavelength in Å, surface brightness *h(BOSZ)*, and theoretical continuum level in the same units as *h(BOSZ)*. While theoretical models often are in units of Eddington flux H where the flux at the stellar surface is

$$F = 4\ \pi\ H, \tag{1}$$

e.g. Sirius from the Kurucz web site[5] and Tremblay et al. (2017). Our *h(BOSZ)* values are four times larger than H, so that

$$F = \pi\ h(BOSZ). \tag{2}$$

The units of our BOSZ flux F emitted at the stellar surface is erg cm^{-2} s^{-1} Å^{-1}, while the Kurucz flux unit is ten times smaller, i.e. erg cm^{-2} s^{-1} nm^{-1}. In order to properly account for limb darkening, the original model calculations produce specific intensity I at 17 angles with respect to the stellar surface. Both *h(BOSZ)* and H are numerical integrals of I over 2π steradians and represent the net out-going flux at optical depth zero according to Equations 1 and 2.

In the absence of interstellar extinction, the total stellar luminosity in erg s^{-1} Å^{-1} is the same at the stellar radius R and at the distance to the Earth r

$$4\ \pi\ R^2\ F = 4\ \pi\ r^2\ f, \tag{3}$$

where f is the measured absolute flux distribution. Thus, the stellar angular diameter is

$$\theta = 2R/r = 2\ \sqrt{f/F}. \tag{4}$$

Figure 2 is an example of the use of the measured CALSPEC flux f for Sirius (Bohlin 2014) along with model atmosphere calculations F to determine the angular diameter. The heavy solid line represents the angular diameter as a function of wavelength using the Kurucz

[5]http://kurucz.harvard.edu/stars/sirius/sirallpr16.500resam501

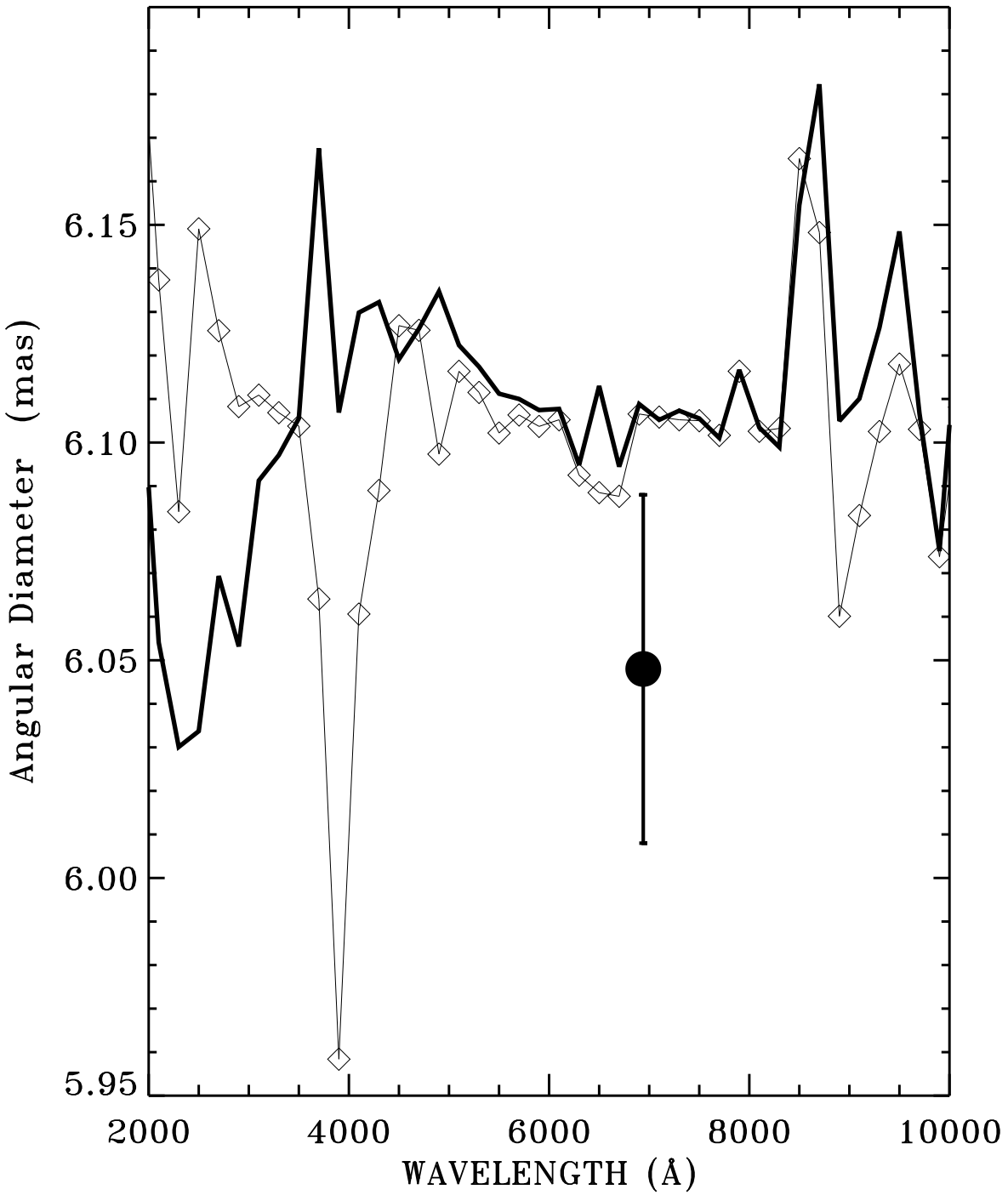

Fig. 2.— Angular diameter of Sirius as a function of wavelength in 200 Å bins. The heavy solid line utilizes the specially constructed model from the Kurucz website; and the thin line with diamonds represents the best fit of our BOSZ models with $T_{\rm eff}$=9820 K, $\log g$=3.95, $[M/H]$=0.45, and E(B-V)=0.000. The interferometric measure of Davis et al. (2011) at 6941 Å is the filled circle with error bar.

model for H with $T_{\rm eff}$=9850 K, $\log g$=4.3, and $[M/H]$=0.4, while the light line with diamonds is the result of fitting the CALSPEC SED with our *h(BOSZ)* grid (see the next section.) The BOSZ fit provides a slightly more constant value of θ, except in the region of the Balmer line confluence, where the exact opacity is not known. Different modeling codes use different approximations to calculate this opacity. The data point is the interferometric measurement of 6.048 mas (Davis et al. 2011) with its 0.04 mas error bar. (Also compare with the discussion in Linnell et al. (2013).) While the Davis et al. (2011) measure agrees with the two results from both models within the 1σ uncertainty, increasing the model surface flux or decreasing the measured absolute CALSPEC flux by ∼1% would reduce the difference. Davis et al. (2011) also discuss other measurements of the angular diameter of 6.039 and 6.089 at 2.2 μm both with a 0.02 mas uncertainty but with questions raised about the validity of the uncertainty for the 6.089 value.

The total volume of the bz2 zipped ASCII version of our new grid is ∼3.7 TB, and access to grid subsets is at the MAST High Level Science Product (HLSP) page for the BOSZ models.

Models can be retrieved in a variety of ways. A web search form allows users to specify one or more parameter selections among $T_{\rm eff}$, $\log(g)$, [M/H], [C/M], [α/M], and/or instrumental broadening. For relatively small numbers of models, users can directly download the ASCII or FITS versions from links in the search results table. For larger numbers of models, users can opt to obtain a wget or cURL script as output, which they can save and then execute on their own machines for sequentially downloading each of the requested files. Users can also download pre-constructed bundles of models for commonly requested sets (e.g., all models at a particular instrumental broadening, or all models at solar relative abundances but differing overall metallicity). For detailed instructions, consult the MAST HLSP page for BOSZ.

4. FITTING MODELS TO OBSERVED SEDs

The model that best fits the observed CALSPEC SED is determined by the minimum chi-square fit of models interpolated from a model atmosphere grid. A set of wavelength bins are selected and the chi-square (χ^2) difference between the data and a model for each bin is computed along with the reduced chi-square average, where the reduction is by the four free parameters of the fit. The expected uncertainties for the χ^2 calculations depend on the amount of line-blanketing in the models, the background noise of the observations, and the broadband repeatability of the observed CALSPEC SEDs for bright stars where the sky background is negligible. The global search for a minimum chi-square proceeds over the

four parameters $T_{\rm eff}$ (10), $\log g$ (0.05), $\log z$ (0.01), i.e. [M/H], and interstellar reddening from the dust E(B-V) (0.001), where the step size of the search in each parameter is in parentheses. With a total to selective extinction ratio at V of 3.1, the extinction curve for interstellar reddening is from Cardelli et al. (1989) below 2 μm and from Chiar & Tielens (2006) above 2 μm, where the Chiar & Tielens (2006) curve is normalized to Cardelli et al. (1989). This composite extinction is multiplied by the selective extinction E(B-V) to get the total extinction A_λ in magnitude units.

The fitted models provide an estimate of IR fluxes beyond the long-wavelength limit of the observation; and the established IR flux standards provide calibration sources for JWST and other IR instrumentation. To limit systematic effects in the modeling and extrapolation process, a variety of stellar types are used for an instrumental flux calibration; and averaging the instrumental sensitivities over several stellar standards of each type provides a statistical reduction of the random errors in the measured fluxes and in the fitting process. For example, observing four stars with a 1% statistical uncertainty each will reduce the uncertainty to 0.5% and will provide a flux calibration on the HST flux scale within the 0.5% statistical uncertainty. Stars cooler than G type are avoided because of the added complication of accounting for the plethora of molecular opacities in their atmospheres.

Table 3 lists the wavelength intervals used for fitting G–F stars, while Table 4 contains the A–O star bins. All bins have equal weight in the fitting process, but the weight of diferent wavelength regions is controlled by the number of bins in each region. The ranges are chosen to avoid some of the stronger absorption lines that may be less accurately modeled. Some UV regions with higher line blanketing are avoided, and the UV regions are generally de-emphasized because of the severe blanketing that makes the models less precise. However to some extent, averaging over broad bins reduces the statistical uncertainties of absorption line strengths in the models. Bins not covered by observed CALSPEC STIS or NICMOS fluxes are omitted, and UV bins with average flux <1% of the peak stellar flux are also not considered. The 1–1.3 μm region is avoided because of larger uncertainties in the NICMOS non-linearity correction of Bohlin et al. (2006). The two bins at the longest wavelengths are not used for P177D, because there is only a single NICMOS G206 observation.

While all of our BOSZ models are available from the MAST Archive, only models with scaled relative solar abundances are considered here, in order to have a proper comparison with the other solar abundance grids discussed in this paper. Possible variations of carbon and α-process elements are deferred to a separate study of fitting with the full BOSZ model composition set. Our technique finds the best χ^2 fits for the wavelength bins of Tables 2–3. Because many stars do not have the NICMOS IR coverage beyond the STIS 1 μm limit, a comparison of the model fits is made with and without the NICMOS data in order to assess

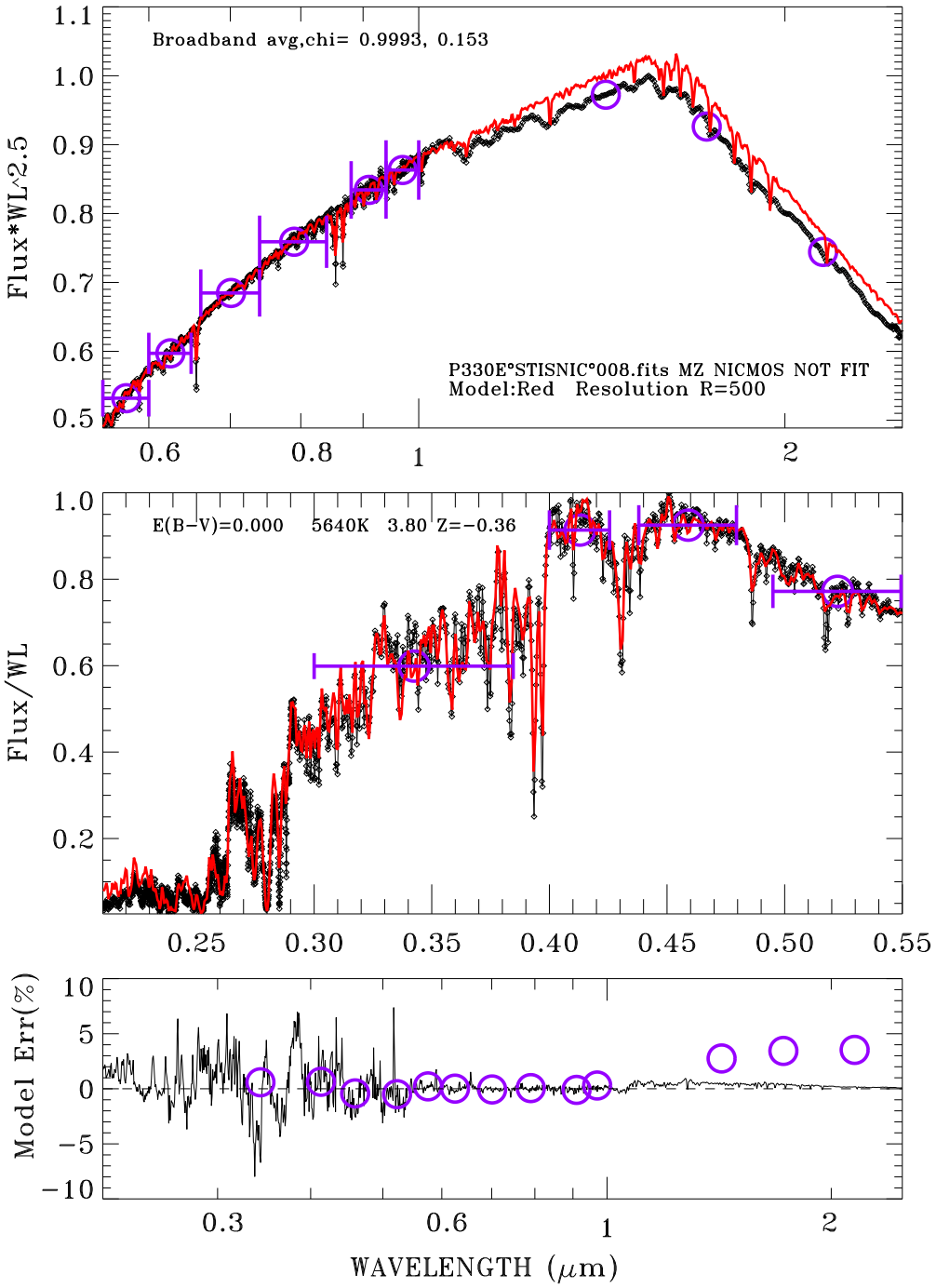

Fig. 3.— BOSZ fit to only the CALSPEC STIS data for P330E. In the top two panels, black is the measured SED with STIS data below the 10100 Å crossover point with NICMOS, while the red model has the parameters on the middle panel. Both model and data are scaled by the same power of wavelength according to the Y-titles. Purple circles represent the data averages in the bins of Table 3 and horizontal error bars are the bin widths. Circles without error bars are the NICMOS averages that are not used in the fitting of the model. The bottom panel shows the residuals to the fits where the black line is the difference between model fit and data on a scale of ±10% of the peak stellar flux. The purple circles are the average binned differences on a scale of ±10% of the local flux.

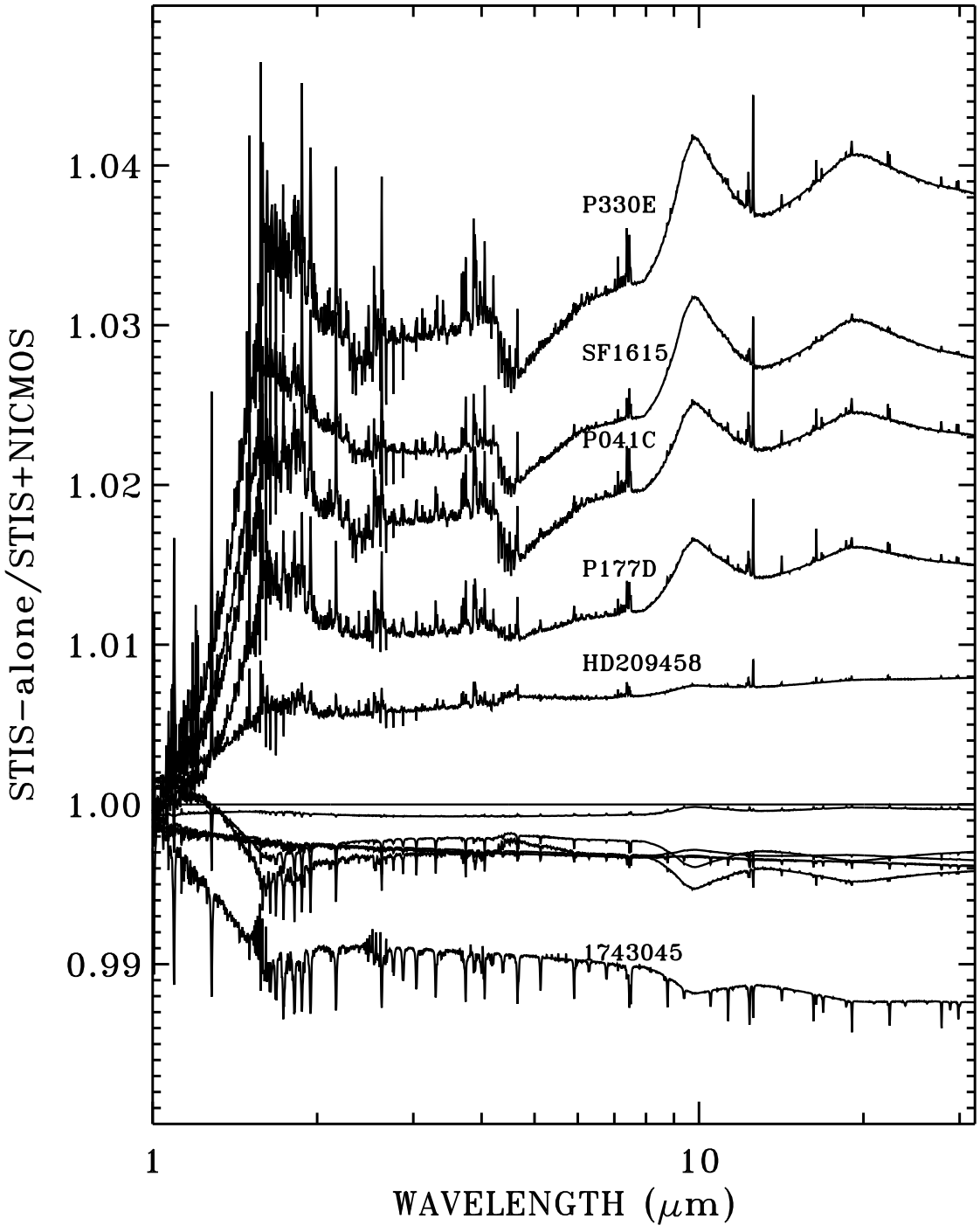

Fig. 4.— Ratios of two independently derived IR SEDs of BOSZ fits to our 13 stars with NICMOS data. The numerators consider the fit to only the STIS portion below 1 μm, and the denominators are the model fits to the full STIS+NICMOS datasets that extend to 2.5 μm. The ratios for the A stars 1802271 and 1812095 fall at unity; and the six outlier ratios are labeled. The remaining two G stars (C26202 and SNAP2) and three A stars (1732526, 1805292, and HD165459) fall between 0.995 and 1.000.

the possible errors for the stars that have only STIS data. The R=500 BOSZ models that approximately match the STIS resolution are used. For the seven G stars and six A stars with NICMOS coverage, the models from the STIS-only fits all agree with the measured NICMOS SEDs within the ∼2% NICMOS uncertainty in all three IR bins, except for P330E and SF1615+001A, where the errors exceed 2% at the 2.5 μm long wavelength limit for NICMOS. For the worst case of P330E with our new model grid, Figure 3 illustrates the STIS-only fit and the residuals. Figure 4 illustrates the IR ratios of the best fit BOSZ models without and with consideration of NICMOS. The ratio for P330E in Figure 4 represents a worst case (perhaps 3σ) uncertainty of our extrapolated IR SEDs. The results for the CK04 and MARCS grids are similar. The BOSZ fit parameters to the P330E STIS+NICMOS data, i.e. $T_{\rm eff}$=5840, $\log g$=4.40, $[M/H]$=-0.16, and E(B-V)=0.036, are from Table 5, while the STIS-only fit parameters are $T_{\rm eff}$=5640, $\log g$=3.8, $[M/H]$=-0.36, and E(B-V)=0.000, i.e. 200 K cooler. This case reflects the partial degeneracy between $T_{\rm eff}$ and reddening E(B-V). Without the constraints of a robust measure of a UV continuum from 1500–3000 Å, a higher $T_{\rm eff}$ is compensated by a higher reddening that produces the same model flux to <1% in all of our G-star bins in the STIS wavelength range. Even with the constraint of the NICMOS SED to 2.5 μm, the chi-square values for the 13 bins of Table 3 range from only 0.1 to 1, which reflects the underconstrained nature of the fitting process. The UV fluxes for G stars are not used as constraints, because even the solar flux is known to vary by more than a percent below 2500 Å. Longer wavelength IR photometry, such as Spitzer/IRAC data would provide additional very helpful contraints.

Nevertheless, the case of P330E most likely represents an extreme error and not a systematic problem with our fits to the STIS-only SEDs. In general, the NICMOS data confirm the STIS-only model fits to ∼2% at the 2.5 μm long wavelength limit for most of the stars with NICMOS spectra. Thus, the expected 1σ uncertainty of our modeled IR fluxes should be of order 1% with respect to the HST flux scale. However, the G stars in Figure 4 include the three outliers P330E, SF1615+001A, and P041C, which are all ∼2% or more high. Thus as a group, the A stars are more reliable IR flux standards than the G stars; and IR standards with NICMOS data are preferred over those with only STIS data, especially in the case of G stars.

5. THE MODEL FITS

5.1. G Stars

Table 5 includes the results for 12 G stars using bins longward of 3000 Å. Over the fitted range, all three grids produce comparable results often with the same $T_{\rm eff}$ to 40 K.

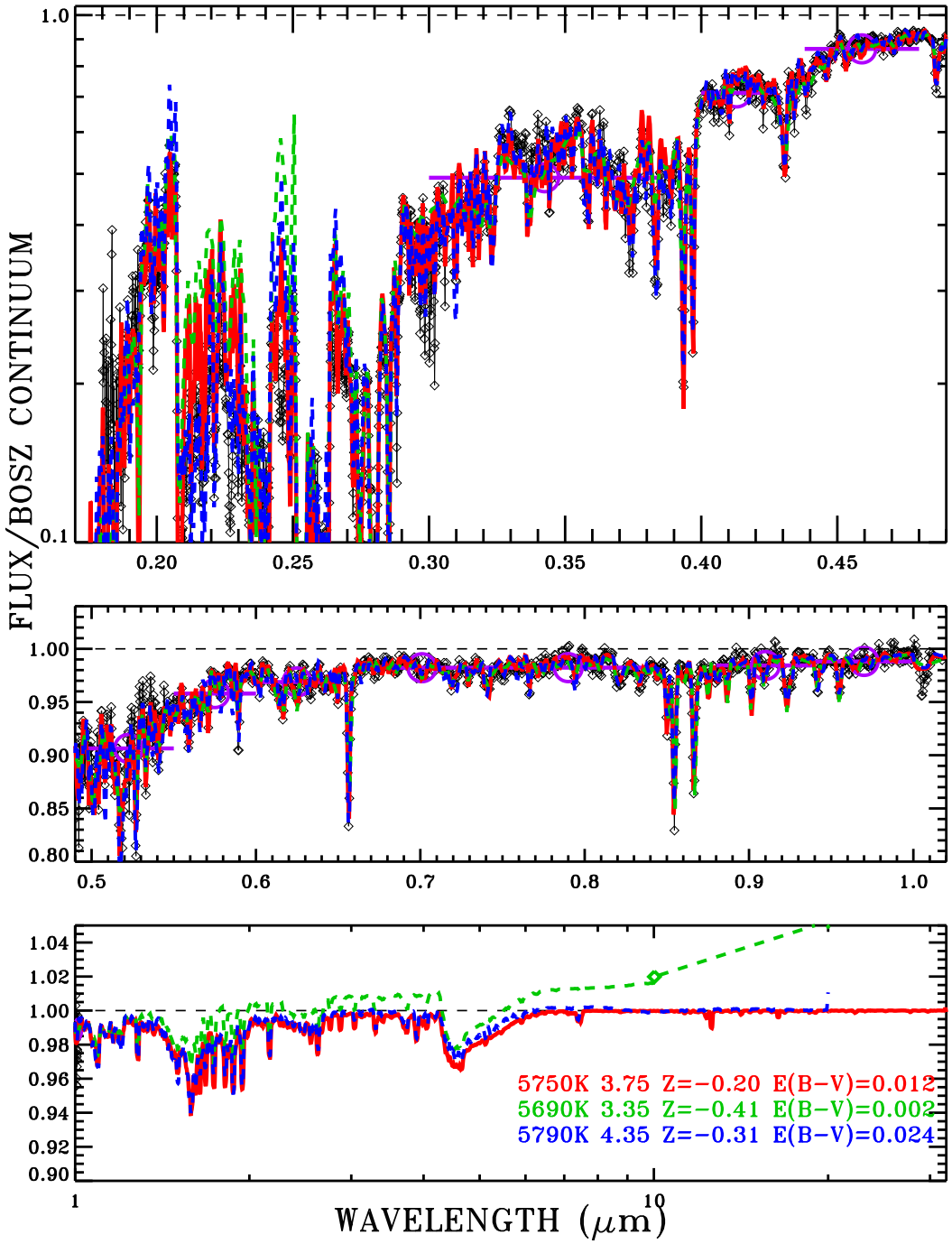

Fig. 5.— The best fitting models for HD37962, where our BOSZ model is red, green dashes represent the CK04 model, and the blue dashed line is the MARCS model. The STIS data are the small black diamonds connected with a thin black line. In the bottom panel, the green diamond point at 10 μm is one of only three CK04 sample points in the entire 10–40 μm range.

From 1-20 μm, the BOSZ and MARCS model fits always agree to $\sim$1%, while the CK04 fits occasionally disagree with the BOSZ by nearly 2%. A worst case is HD37962, where the CK04 fit approaches 2% higher than the BOSZ fit at 10 μm, as shown in Figure 5. From 10–40 μm there are only three tabulated CK04 flux values, which are not very useful for comparing with observation in the mid-IR.

The six G stars with UV data below 3000 Å are compared to the short wavelength extensions of their models in Figure 6. Below 3000 Å, line-blanketing removes over half of the continuum flux, making modeling problematic because of our incomplete knowledge of the physical parameters of the atomic lines. Thus, occasional deviations of the models from the data by a factor of two is not surprising. However, the quality of the fits might depend on deviations of the carbon and α-process elements from the solar abundance assumed for the models in Figure 6.

No model matches the data to 20% over the entire 2000–3000 Å range of Figure 6. However, the MARCS models match the data from 2700–3000 Å and to 30% over most of the range, except for P330E. The quality of our BOSZ fits is comparable to MARCS, while the CK04 fits tend to be the outliers. All three models are always higher than the data in the 2650 Å region for all six stars, although the BOSZ models have only about half the error of the other two fits.

5.2. A–O Stars

Table 6 includes the results for both our BOSZ and the CK04 grids for the 19 stars that are hotter than 7000 K. The $T_{\rm eff}$ results for the two cases all agree to 40 K, except for HD158485 with a difference of 60 K. There are six stars with $T_{\rm eff}$ below the MARCS upper limit of 8000 K; and the MARCS fits are systematically cooler than our BOSZ results by by 50–100 K. This systematic difference just means that the same SED shape is labeled as cooler in this temperature range of the MARCS grid, but both grids provide equally valid results. The models in the line-free regions agree to 1% for the comparison of BOSZ to CK04 out to 10 μm, while the BOSZ and MARCS fits also agree to 1% to the 20 μm limit of the MARCS grid. This consistency reinforces the above suggestion that our BOSZ extrapolations have a 1σ uncertainty of order 1% in the IR.

At higher $T_{\rm eff}$, Lanz & Hubeny (2003) for $T_{\rm eff}$ 27,500–55,000 K and Lanz & Hubeny (2007) for $T_{\rm eff}$ 15,000–30,000 K compute NLTE model grids, which better represent the physics of the hottest stellar atmospheres than LTE models. These NLTE Lanz models are

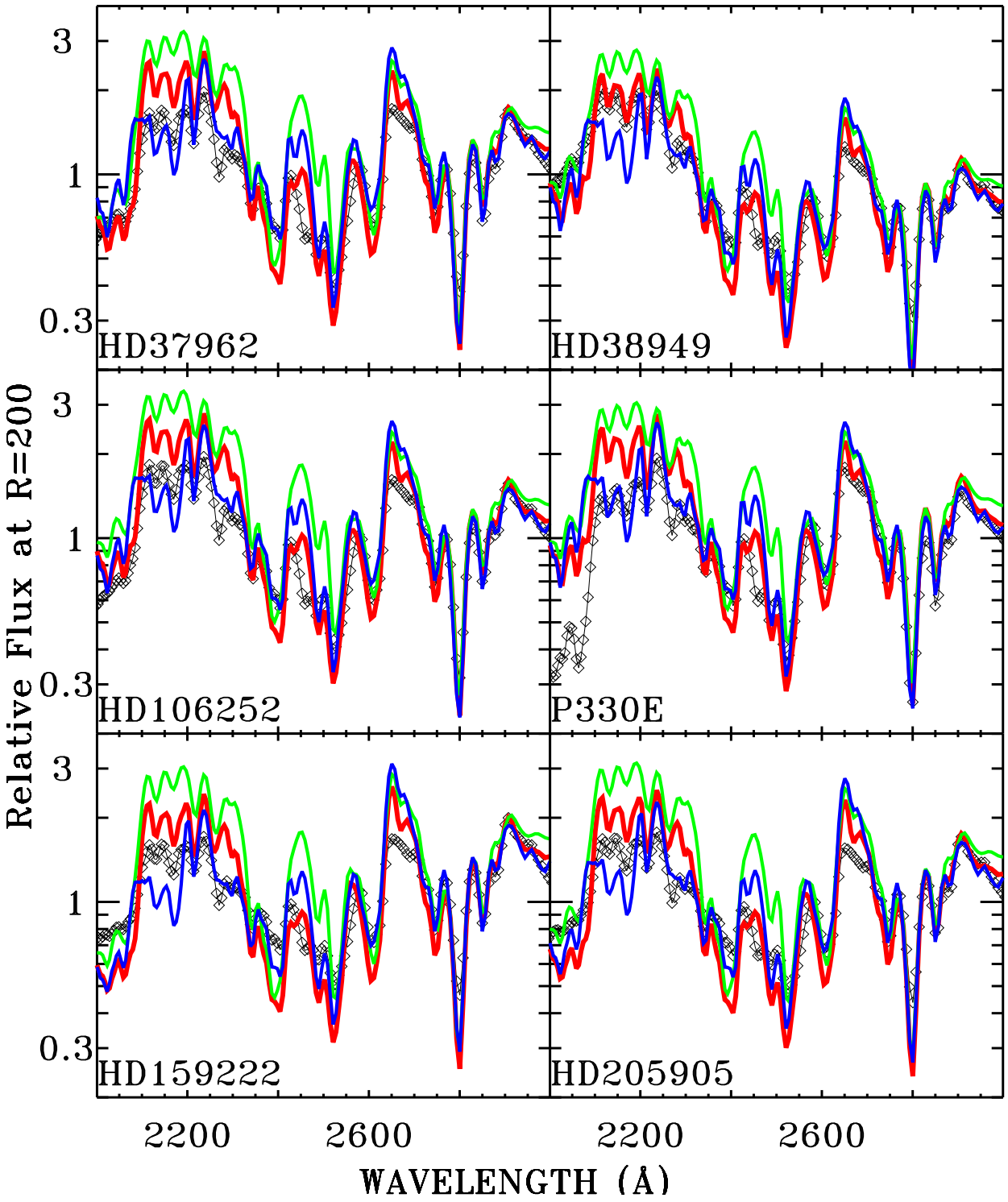

Fig. 6.— Black diamonds: STIS UV fluxes for six G stars. Models: Red–BOSZ, Green–CK04, Blue–MARCS. All three models from Table 5 and the STIS data are smoothed to a resolution R=200. The models are normalized to STIS at 6800–7700Å. Both data and models are divided by the wavelength to the 8th power for display.

binned in frequency and merged into the CLOUDY format in the file *obstar_merged_3d.ASCII.gz*[6]. Above $T_{\rm eff} = 15,000$, the NLTE models characterize our three O stars, where the best fits are summarized in Table 7. The modeled NLTE strengths of Paschen absorption lines are particularly sensitive to the parameters of the fits, so two wavelength bins at 9549 and 9232 Å (vacuum) for Pϵ and P9 are included in Table 4 in order to improve the fits to the Paschen equivalent widths. Not only does the line structure often match the data better in the Figure 7 example, but also the χ^2 is up to a factor of two better for the Lanz OB-star grid.

For the three stars with $T_{\rm eff}$ above the 15,000 K lower limit of the OB-star NLTE grid, the NLTE IR fluxes longward of 1 μm are systematically higher than the LTE grid fits. The worst case IR difference is for λ Lep as illustrated in Figure 8, where the best fitting BOSZ and Lanz models differ by 11% at 32 μm. While there are no CALSPEC stars near the 15,000 K lower limit of the Lanz grids, a proper comparison beween LTE and NLTE at this cross-over point is accomplished by fitting the Lanz $T_{\rm eff}$=15,000, $\log g$=3.5, and $[M/H]$=0 model with our BOSZ grid over our usual range of Table 4. The best BOSZ fit is $T_{\rm eff}$=14,980, $\log g$=4.0, and $[M/H]$=-0.36. While the two models differ slightly in their parameter labels, the important difference is in the IR fluxes, as illustrated in Figure 9. A comparison using the same $T_{\rm eff}$=15,000, $\log g$=3.5, and $[M/H]$=0 BOSZ model shows a slightly worse discrepancy. Unfortunately, the NLTE model has systematically higher flux in the IR with an 8% divergence at 32 μm. Either there is some deficiency in the LTE or NLTE model calculations, or NLTE is important in the mid-IR below 15,000 K. One suspicious aspect of Figure 9 is that the NLTE model shows no Brackett, Pfund, or higher hydrogen line series converging to their continuum discontinuities like both models at the 0.82 μm Paschen limit. Perhaps, the problem is just that the NLTE Lanz models utilize an incomplete model hydrogen atom. In any case, there is evidence that LTE models have no problem below 10,000 K, where Bohlin (2014) found one percent average agreement between a special LTE Kurucz model at 9850 K for Sirius[7] and MSX absolute flux measures at 8, 12, 15, and 21 μm. Futhermore, a fit of BOSZ models to this special Kurucz model for Sirius is consistent with <1% difference at 32 μm.

[6]nova.astro.umd.edu/Tlusty2002/tlusty-frames-cloudy.html

[7]http://kurucz.harvard.edu/stars/sirius/

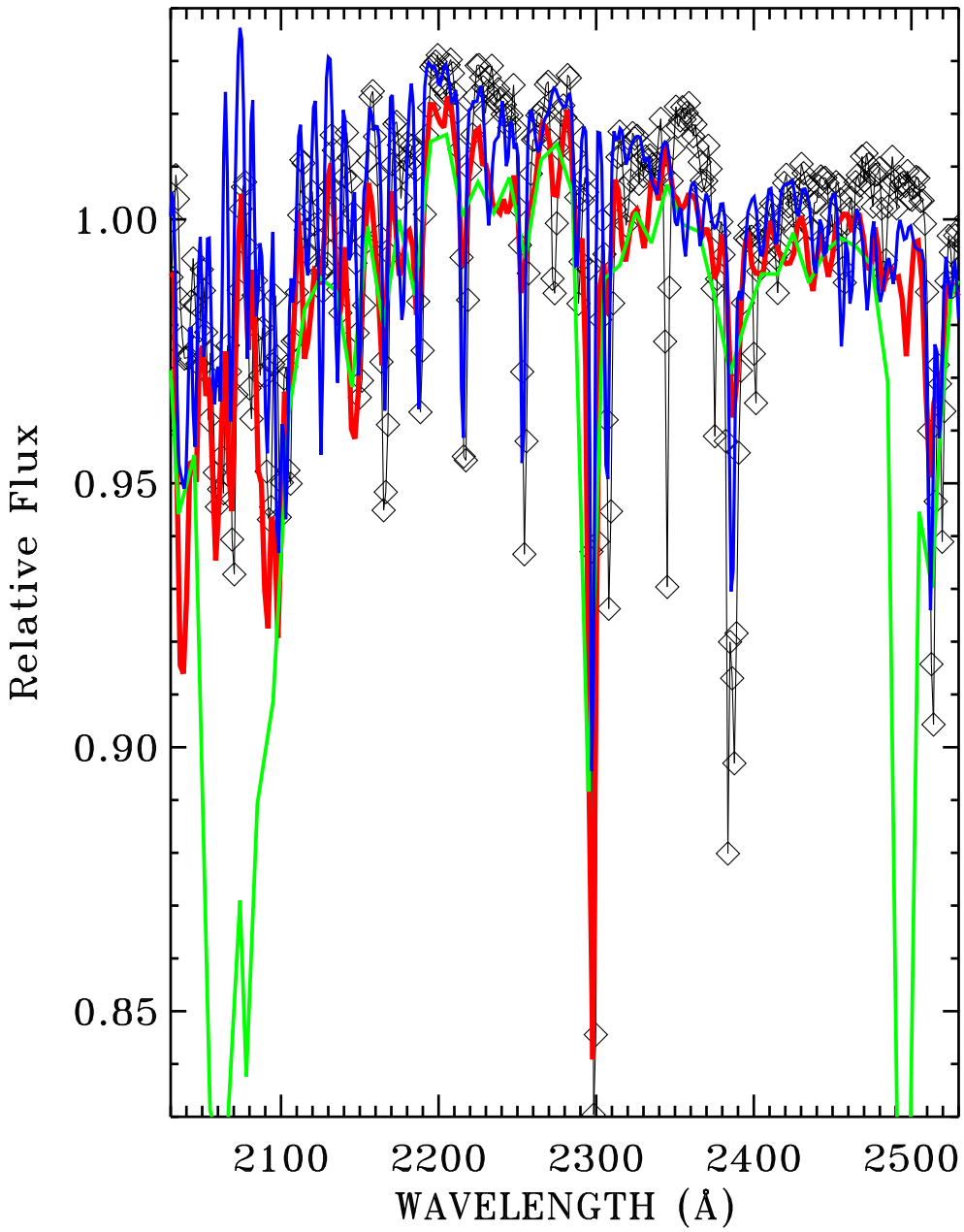

Fig. 7.— STIS and modeled fluxes for μ Col as in Figure 6, except that the resolution is R=500 and the scaling is by wavelength cubed. The STIS data are the black diamonds connected with a thin black line. Our BOSZ model is red, and the blue line is from the (Lanz & Hubeny 2007) B-star grid. The solid green line illustrates the two erroneous CK04 features.

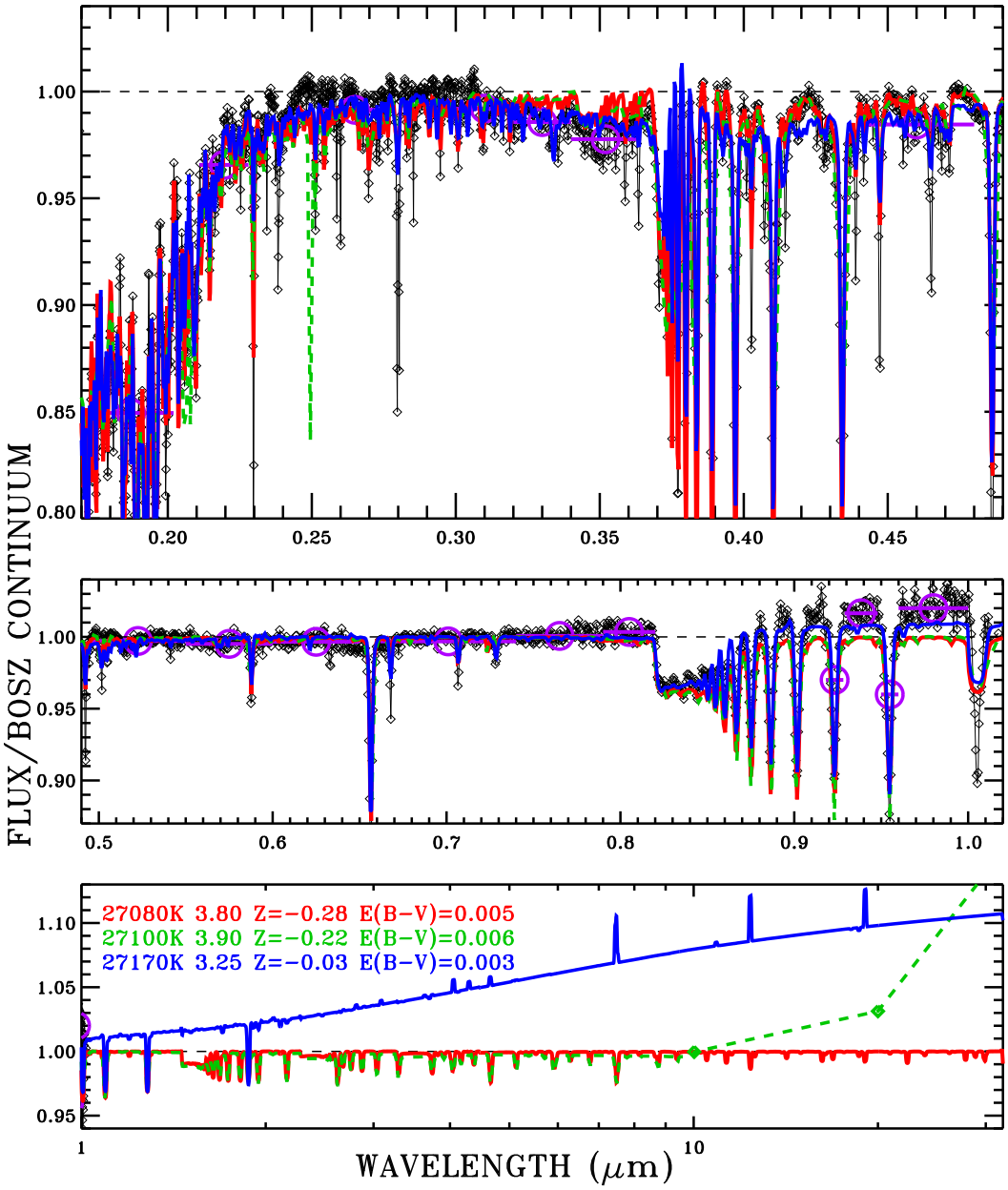

Fig. 8.— As in Figure 5 for λ Lep, where the STIS data are the black diamonds connected with a thin black line, our BOSZ model is red, CK04 is green, and the blue line is for the Lanz B-star NLTE grid. Despite agreement of the data with all three models to ∼2% in broad bins, the NLTE grid fit differs systematically from the two LTE grid fits in the IR. The NLTE model fits the STIS SED significantly better in the continuum between the Paschen lines at 0.9–1μm.

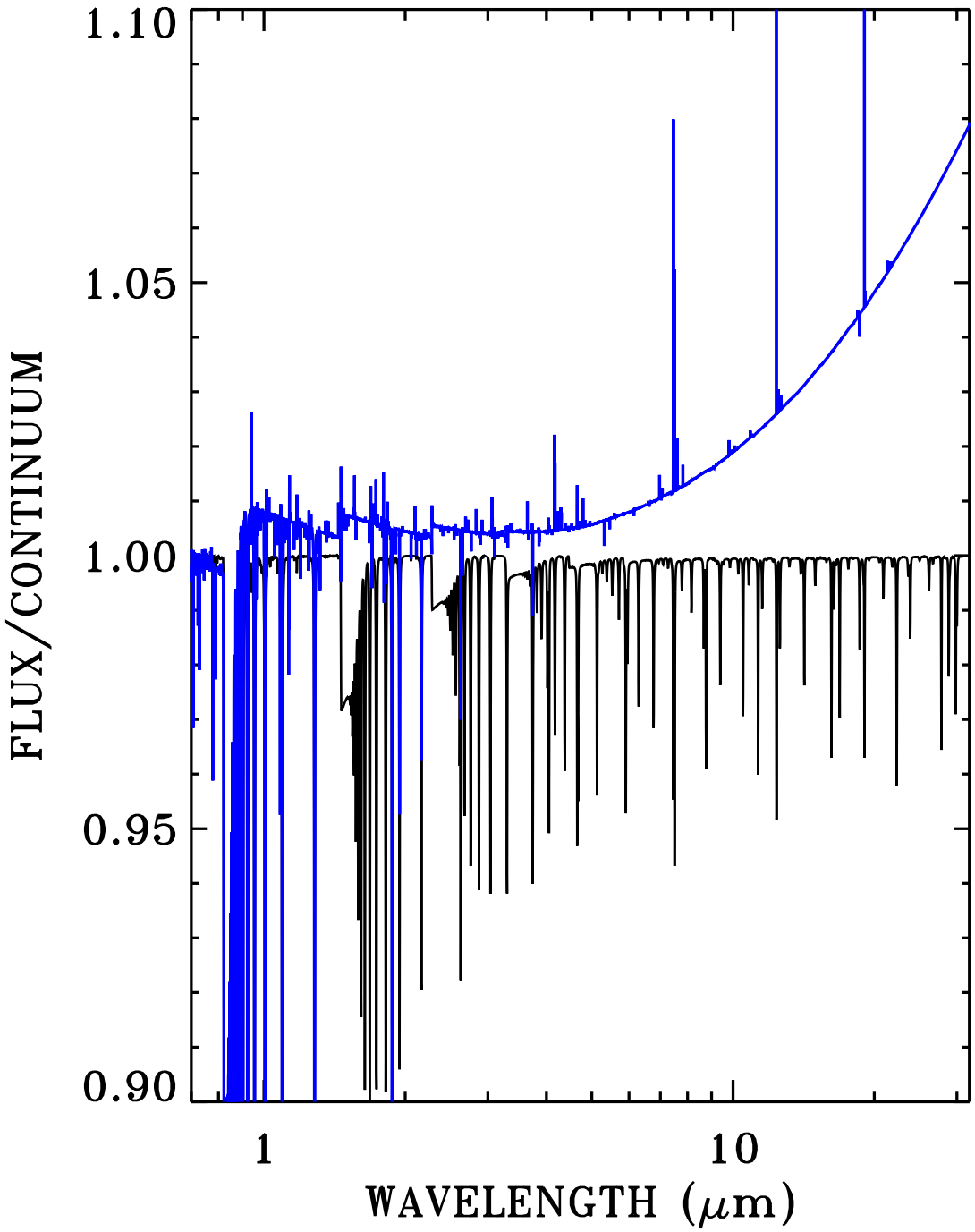

Fig. 9.— Comparison in the IR of a Lanz NLTE model (blue) at 15,000 K to the best fitting a BOSZ LTE model (black). The two models are normalized at 6900–7700 Å and are matched in the bins of Table 4. Both models are divided by the BOSZ continuum, which is normalized by the same factor as the model normalization. Unfortunately, the NLTE model is systematically more than 1% brighter longward of 5 μm and rises to almost an 8% deviation at 32 μm.

5.3. K Star

While the proposed JWST standard stars are type G and hotter, there is one K1.5III CALSPEC star KF06T2 (a.k.a. 2MASS J17583798+6646522). The model fits for the BOSZ, CK04, and MARCS grids all match the measured KF06T2 fluxes below the 2.5 μm NICMOS limit but diverge by more than 2% longward of 10 μm, as shown Figure 10. The precision of the IR K-star fluxes is probably worse than for the hotter stars because of the difficulty of modeling the strong molecular bands, especially for CO near 2.4 and 4.6 μm.

5.4. An Alternate Method, i.e. Fitting Balmer Lines

The discussion above is about fitting broad regions of the stellar continuum to determine the $T_{\rm eff}$, $\log g$, and $[M/H]$. However, fitting the Balmer line profiles provides an independent check on the temperature and gravity, although the hydrogen line shapes are not very sensitive to metallicity. Figure 11 exemplifies the challenges of fitting high resolution spectra for the Hβ region in HD14943 (A5V). The myriad narrow metal lines complicate automated fitting of the models to real data, as illustrated in Figure 11. Even though the MARCS models are monochromatic samples at R=20,000 and miss many narrow lines between sample points (Plez 2008), the MARCS and BOSZ show nearly perfect agreement for the overall shape of the broad Hβ line. The BOSZ and CK04 SEDs represent the mean flux in bandpasses defined by the sample spacings. Cooler stars with narrower Balmer lines have higher densities of confusing lines. Another caution is that the Balmer line cores are formed high in the atmosphere, where the plane-parallel modeling assumption may break down and render the central regions of the modeled Balmer lines unreliable. However, the good agreement of the MARCS R=20,000 resolution with the BOSZ R=300,000 suggests that 20,000 is sufficient for a ground-based observational program. Furthermore, the good agreement of the STIS data with the R=500 model demonstrates that any higher resolution data should also agree to first order with a high resolution model. For our hottest stars, a NLTE grid of high resolution Balmer profiles would be required. For a NLTE/LTE grid of Balmer line profiles and a discussion of the effects of stellar rotation on the line profiles, see González Delgado & Leitherer (1999). Thus, an observing program to obtain high resolution spectra of the Balmer lines could verify our derived $T_{\rm eff}$ and $\log g$, provided the stellar rotational velocity is low and provided that the central core of the model line profiles precisely represents the true conditions in the outer fringes of stellar atmospheres.

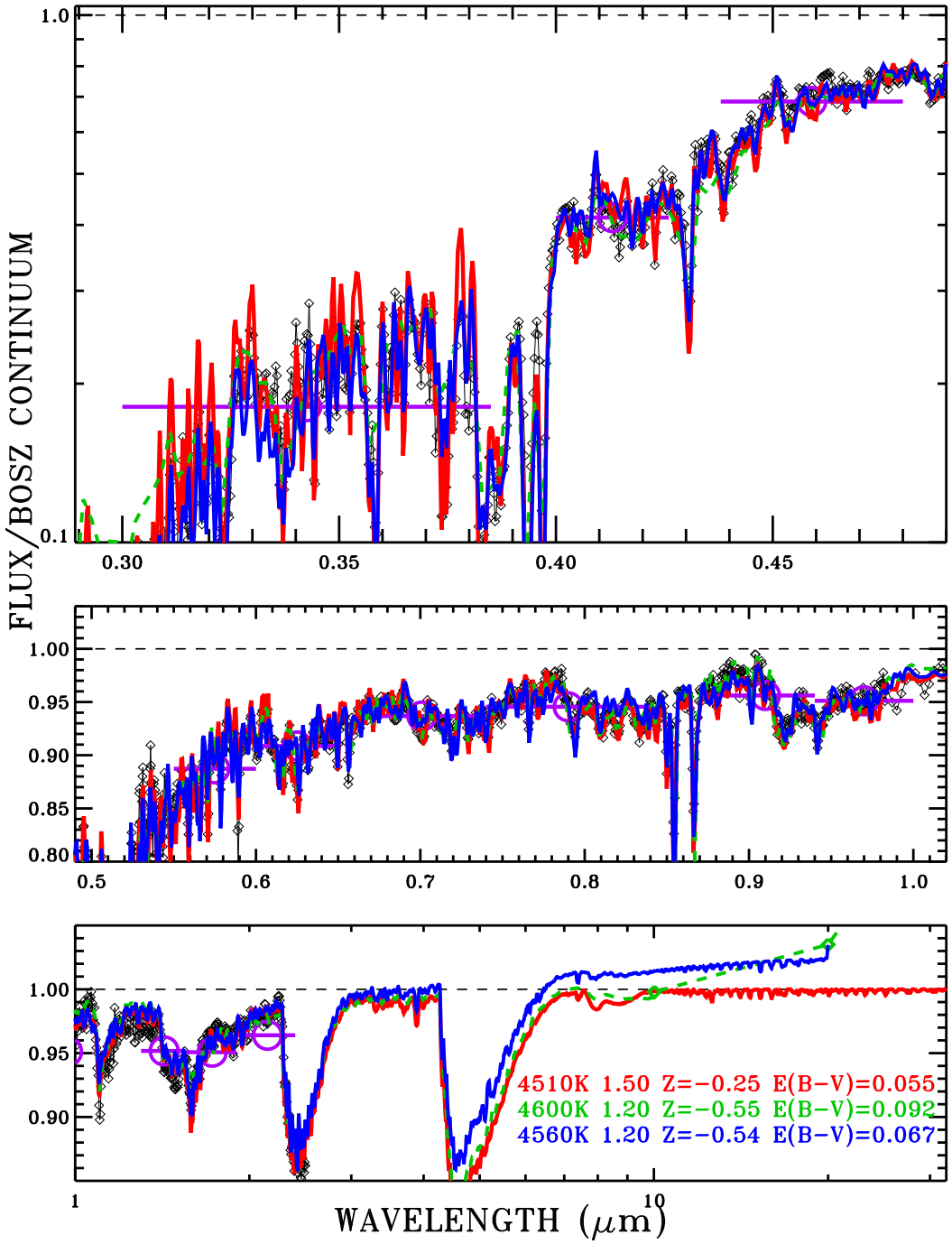

Fig. 10.— As in Figure 5 for $KF06T2$, where the STIS and NICMOS data are the black diamonds connected with a thin black line, our BOSZ model is red, CK04 is green, and Marcs is the blue line. Despite agreement of the data with all three models, there is more than a 2% disparity among the models in the IR. Notice the strong molecular band structure in the bottom panel.

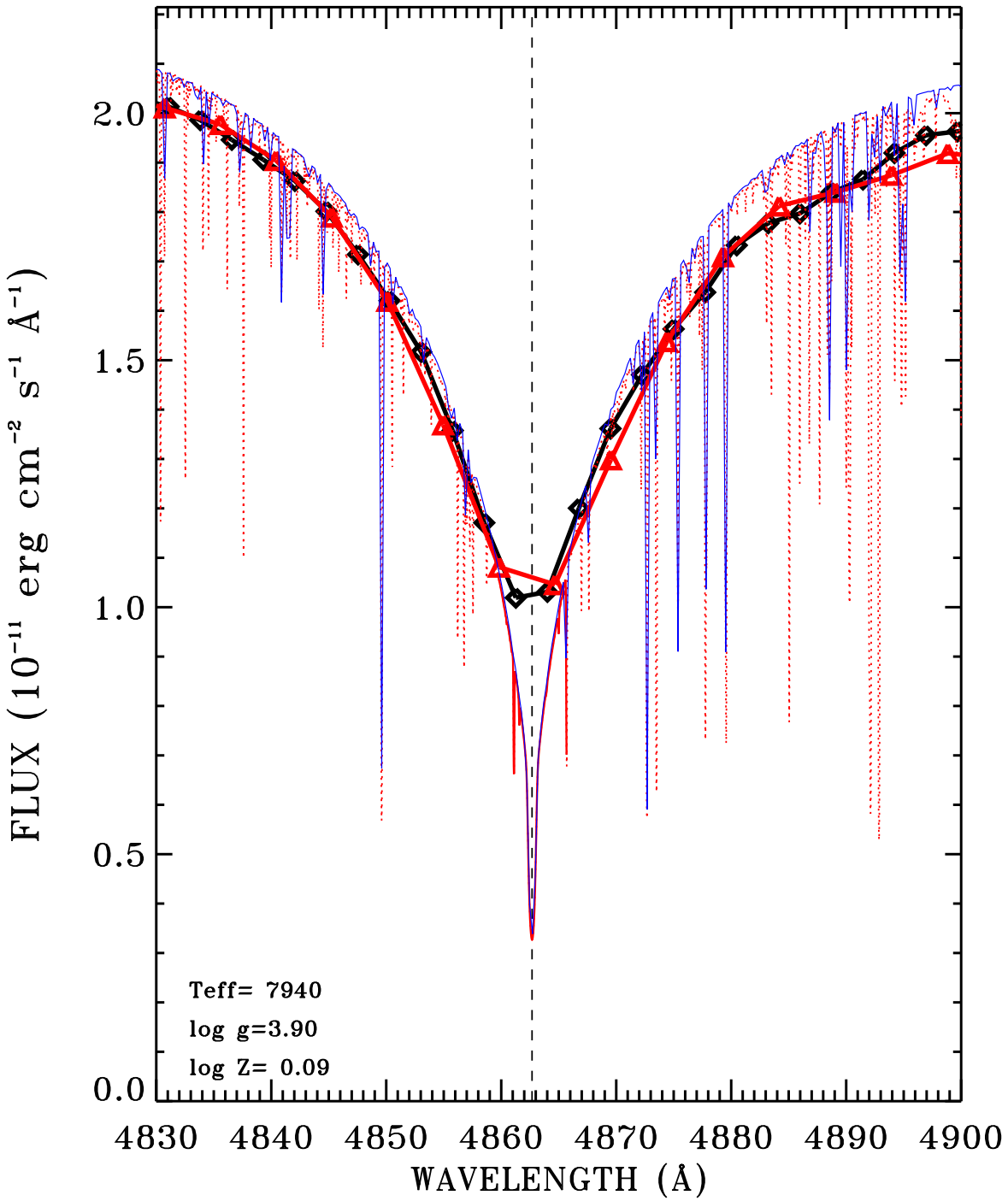

Fig. 11.— Hβ region for HD14943 on a vacuum wavelength scale. Black heavy line and diamonds are the STIS observations at a resolution R that is between 500 and 1000, while the heavy red line and triangles are the best fit R=500 BOSZ model with the Table 6 parameters that are written on the plot. The thin red dotted line that is solid near line center is the BOSZ R=300,000 model, and the thin blue line is the MARCS R=20,000 model with its best fit of $T_{\rm eff}$=7930 K, $\log g$=3.90, $[M/H]$=0.07, and E(B-V)=0.012. All models are normalized to the STIS flux at 6800–7700 Å.

6. CONCLUSIONS

Our new comprehensive set of model atmospheres are now publically available through the MAST[8] at the Space Telescope Science Institute and have a wavelength coverage of 0.1–32 μm with an extensive variety of chemical composition, stellar temperature, and gravity. The wavelength coverage and properly sampled SEDs with 10 spectral resolutions R in the range of 200–300,000 are essential to the flux calibration and interpretation of stellar spectra from the James Webb Space Telescope. No comparable sets of model spectra are publically available. Our new BOSZ grid fits the STIS and NICMOS flux distributions well with $\chi^2 = 0.1$–3 for most of our stars, which have $T_{\rm eff} < 15,000\ K$.

The CK04 LTE models for the three hottest stars have two spurious strong UV features that are corrected in our new model grid, as illustrated for μ Col in Figure 7. One erroneous feature is excess continuum absorption from the HeII Paschen limit at 2050.6 Å (vacuum), while the extraneous 2496.8 Å absorption is a single line of OIII with an overestimated line strength.

The Lanz NLTE models are used to establish the IR SEDs of our three hottest stars; but unfortunately, these NLTE models do not converge to their LTE counterparts at 15,000 K, as expected. The problem may lie with an incomplete modeling of the higher atomic hydrogen lines in the Lanz grid. However, the complete SEDs of our cooler standards that are derived from χ^2 fits of our BOSZ models to the measured HST flux distribution have an expected 1σ uncertainty of $\sim$1% to their long wavelength limit of 32 μm. The HST fluxes at the shorter wavelengths are concatenated with their best fit R=500 BOSZ model at the longer wavelengths and are available in the CALSPEC public database. The complete R=300,000 model SEDs also reside in CALSPEC[9]. Perhaps, the most significant improvement in our predicted IR SEDs could come from new constraints provided by Spitzer/IRAC photometry of our stars.

Primary support for this work was provided by NASA through the Space Telescope Science Institute, which is operated by AURA, Inc., under NASA contract NAS5-26555. Szabolcs Mészáros has been supported by the Premium Postdoctoral Research Program of the Hungarian Academy of Sciences and by the Hungarian NKFI Grants K-119517 of the Hungarian National Research, Development and Innovation Office. A part of the computations were run on the 'atlasz' cluster of the Eotvos Lorand University, Budapest. We acknowledge

[8] `https://archive.stsci.edu/prepds/bosz`

[9] http://www.stsci.edu/hst/observatory/crds/calspec.html

NIIF Institute for awarding us access to resource based in Hungary at Budapest. Special thanks to Robert Kurucz for his advice and making public his lifetime legacy of the best LTE model atmosphere codes and and related databases. We thank Fiorella Castelli for her guidance during the automatization of SYNTHE. This research made use of the SIMBAD database, operated at CDS, Strasbourg, France

A. Model Naming Convention

The naming convention for the models is explained using the example amp05cp00op05t4500g05v20modrt0b500rs, where the first letter is always "a" meaning that the source is an ATLAS model.

mp05: abundance of metals [M/H] (mp if the [M/H] is positive, mm if negative.) The two digits indicate the value of 10[M/H], where 02.5 is rounded to 03, 07.5 to 08, etc. only in the naming conventions.

cp00: carbon abundance [C/M] (cp if the [C/M] is positive, cm if negative.) The digits indicate the rounded value of 10[C/M].

op05: alpha element abundance [A/M] (op if [A/M] is positive, om if negative.) The digits indicate the rounded value of the 10[A/M].

t4500: The effective temperature in K.

g05: The surface gravity, where the digits are the rounded value of the 10log g.

v20: The microturbulent velocity, this is always v20, ie 2km/s.

mod: parameters after this enter only the synthesis.

rt0: The rotational broadening, vrot is always 0.

b500: The spectral resolution R.

rs: The spectra are resampled at two points per resolution element.

Table 3. Broad Bands for Fitting G–F Star Models

Wavelength Range (Å)
3000–3850
4000–4260
4380–4800
4950–5500
5500–6000
6000–6500
6620–7400
7400–8400
8800–9400
9400–10000
13000–15500
15500–19000
19000–24000

Table 4. Broad Bands for Fitting A-B-O Star Models

Wavelength Range (Å)
1280–1510
1725–2020
2110–2280
2520–2780
3000–3200
3200–3400
3400–3640
3750–4400
4400–4800
4950–5500
5500–6000
6000–6500
6620–7400
7400–7900
7900–8200
9182–9282
9290–9480
9499–9599
9600–10000
13000–15500
19700–21400
21900–24000

REFERENCES

Anders, E., & Grevesse, N. 1989, Geochim. Cosmochim. Acta, 53, 197

Asplund, M., Grevesse, N., & Sauval, A. J. 2005, in Astronomical Society of the Pacific Conference Series, Vol. 336, Cosmic Abundances as Records of Stellar Evolution and Nucleosynthesis, ed. T. G. Barnes, III & F. N. Bash, 25

Asplund, M., Grevesse, N., Sauval, A. J., & Scott, P. 2009, ARA&A, 47, 481

Bohlin, R. C. 2010, AJ, 139, 1515 (B10)

—. 2014, AJ, 147, 127

Bohlin, R. C., & Cohen, M. 2008, AJ, 136, 1171

Bohlin, R. C., Gordon, K. D., & Tremblay, P.-E. 2014, PASP, 126, 711 (B14)

Bohlin, R. C., & Proffitt, C. R. 2015, Improved Photometry for G750L, Instrument Science Report, STIS 2015–01, (Baltimore: STScI), Tech. rep.

Bohlin, R. C., Riess, A., & de Jong, R. 2006, NICMOS Count Rate DependentNon-Linearity in G096 and G141, Instrument Science Report, NICMOS 2006–02, (Baltimore: STScI), Tech. rep.

Bohlin, R. C., Gordon, K. D., Rieke, G. H., et al. 2011, AJ, 141, 173

Cardelli, J. A., Clayton, G. C., & Mathis, J. S. 1989, ApJ, 345, 245

Castelli, F., & Kurucz, R. L. 2003, in IAU Symposium, Vol. 210, Modelling of Stellar Atmospheres, ed. N. Piskunov, W. W. Weiss, & D. F. Gray, 20P (CK04)

Chiar, J. E., & Tielens, A. G. G. M. 2006, ApJ, 637, 774

Coelho, P. R. T. 2014, MNRAS, 440, 1027

Davis, J., Ireland, M. J., North, J. R., et al. 2011, PASA, 28, 58

Gilliland, R. L., & Rajan, A. 2011, WFC3 UVIS High-resolution Imaging Performance, Instrument Science Report, WFC3 2011–03, (Baltimore:STScI), Tech. rep.

González Delgado, R. M., & Leitherer, C. 1999, ApJS, 125, 479

Grevesse, N., Asplund, M., & Sauval, A. J. 2007, Space Sci. Rev., 130, 105

Grevesse, N., & Sauval, A. J. 1998, Space Sci. Rev., 85, 161

Gustafsson, B., Edvardsson, B., Eriksson, K., et al. 2008, A&A, 486, 951

Kurucz, R. L. 1979, ApJS, 40, 1

Kurucz, R. L., & Avrett, E. H. 1981, SAO Special Report, 391

Lanz, T., & Hubeny, I. 2003, ApJS, 146, 417

—. 2007, ApJS, 169, 83

Linnell, A. P., DeStefano, P., & Hubeny, I. 2013, AJ, 146, 68

Megessier, C. 1995, A&A, 296, 771

Mészáros, S., Allende Prieto, C., Edvardsson, B., et al. 2012, AJ, 144, 120

Partridge, H., & Schwenke, D. W. 1997, J. Chem. Phys., 106, 4618

Plez, B. 2008, Physica Scripta Volume T, 133, 014003

Price, S. D., Paxson, C., Engelke, C., & Murdock, T. L. 2004, AJ, 128, 889

Rauch, T., Werner, K., Bohlin, R., & Kruk, J. W. 2013, A&A, 560, A106

Sbordone, L., Bonifacio, P., Castelli, F., & Kurucz, R. L. 2004, Memorie della Societa Astronomica Italiana Supplementi, 5, 93

Schwenke, D. W. 1998, Faraday Discussions, 109, 321

Tremblay, P.-E., Gentile-Fusillo, N., Raddi, R., et al. 2017, MNRAS, 465, 2849

Zwitter, T., Castelli, F., & Munari, U. 2004, VizieR Online Data Catalog, 341, 71055

Table 5. Parameters of the Model Fits for G Stars

Star	$T_{\rm eff}$ BOSZ	$\log g$	$[M/H]$	E(B-V)	χ^2	$T_{\rm eff}$ CK04	$\log g$	$[M/H]$	E(B-V)	χ^2	$T_{\rm eff}$ MARCS	$\log g$	$[M/H]$	E(B-V)	χ^2
C26202	6300	4.65	-0.39	0.069	0.51	6320	4.60	-0.45	0.073	0.48	6320	4.85	-0.49	0.076	0.52
HD37962	5750	3.75	-0.20	0.012	0.28	5690	3.35	-0.41	0.002	0.18	5790	4.35	-0.31	0.024	0.35
HD38949	5990	4.30	-0.11	0.001	0.08	5980	4.00	-0.25	0.001	0.07	5990	4.60	-0.26	0.005	0.18
HD106252	5830	3.85	-0.11	0.000	0.17	5820	3.50	-0.28	0.000	0.16	5810	4.20	-0.27	0.000	0.21
P041C[a]	5960	4.15	0.11	0.022	0.17	6040	4.00	0.05	0.040	0.30	6030	4.70	0.02	0.040	0.22
P177D	5850	3.65	-0.02	0.045	0.21	5880	3.45	-0.14	0.053	0.31	5910	4.20	-0.10	0.061	0.26
SF1615+001A	5820	4.45	-0.61	0.105	0.43	5880	4.20	-0.69	0.118	0.60	5860	4.85	-0.77	0.116	0.74
SNAP2	5750	4.40	-0.19	0.033	0.11	5810	4.10	-0.28	0.047	0.12	5800	4.75	-0.32	0.048	0.26
P330E	5840	4.40	-0.16	0.036	0.32	5900	4.10	-0.25	0.049	0.49	5900	4.75	-0.29	0.052	0.52
HD159222	5800	3.55	0.08	0.000	0.16	5790	3.30	-0.09	0.001	0.12	5780	4.10	-0.07	0.001	0.19
HD205905	5850	3.75	0.03	0.003	0.18	5830	3.45	-0.14	0.001	0.14	5870	4.30	-0.08	0.011	0.18
HD209458[b]	6090	4.15	0.01	0.002	0.13	6160	4.05	-0.04	0.017	0.18	6150	4.55	-0.07	0.017	0.20

[a]P041C has an M companion 0.57arcsec away (Gilliland & Rajan 2011)

[b]Transiting planet. See B10.

Table 6. Parameters of the Model Fits for OBA Stars

Star	$T_{\rm eff}$ BOSZ	$\log g$	$[M/H]$	E(B-V)	χ^2	$T_{\rm eff}$ CK04	$\log g$	$[M/H]$	E(B-V)	χ^2
10 Lac	30950	3.90	0.00	0.075	3.27	30910	3.95	0.10	0.077	2.92
λ Lep	27080	3.80	-0.28	0.005	3.52	27100	3.90	-0.22	0.006	3.40
μ Col	30980	4.25	0.20	0.009	3.52	30950	4.35	0.32	0.011	3.34
ξ^2 Cet	10370	3.95	-0.62	0.000	2.85	10370	3.95	-0.52	0.000	1.97
HD014943	7940	3.90	0.09	0.011	0.76	7930	3.90	0.07	0.012	1.04
HD37725	8350	4.25	-0.10	0.041	1.17	8380	4.30	-0.08	0.045	1.43
HD116405	10790	4.00	-0.35	0.000	0.61	10790	4.05	-0.37	0.000	0.42
BD+60°1753	9370	3.90	-0.09	0.013	0.84	9410	3.90	-0.06	0.017	1.01
HD158485	8580	4.15	-0.39	0.046	1.47	8640	4.20	-0.35	0.052	1.72
1732526	8630	4.10	-0.32	0.036	2.92	8670	4.15	-0.25	0.039	2.99
1743045	7470	3.65	-0.29	0.026	1.38	7460	3.65	-0.31	0.026	1.59
HD163466	7960	3.75	-0.21	0.031	2.21	7950	3.75	-0.24	0.031	2.53
1757132	7640	3.75	0.19	0.036	0.83	7660	3.80	0.18	0.041	1.23
1802271	9040	4.00	-0.48	0.017	0.94	9070	4.00	-0.47	0.020	0.98
1805292	8570	4.00	-0.07	0.034	0.80	8540	4.00	-0.11	0.032	0.90
1808347	7910	3.85	-0.61	0.024	2.46	7890	3.85	-0.62	0.022	2.80
1812095	7810	3.65	0.22	0.008	0.88	7830	3.70	0.22	0.013	0.95
HD180609	8560	3.95	-0.44	0.037	0.59	8600	4.00	-0.45	0.042	0.75
HD165459[a]	8570	4.20	0.10	0.023	0.53	8540	4.20	0.07	0.021	0.64

[a]There is a dust ring that affects the SED longward of 8 μm. See Bohlin et al. (2011).

Table 7. Parameters of the Lanz & Hubeny Model Fits for O Stars

Star	$T_{\rm eff}$	$\log g$	$[M/H]$	E(B-V)	χ^2
10 Lac	32190	3.65	0.05	0.071	3.20
λ Lep	27170	3.25	-0.03	0.003	1.94
μ Col	31640	3.65	0.13	0.001	1.76